Structural basis for the activation mechanism of the PlcR virulence regulator by the quorum-sensing signal peptide PapR

Rosa Grenha[a], Leyla Slamti[b], Magali Nicaise[c], Yacine Refes[b], Didier Lereclus[b], and Sylvie Nessler[a,c,1]

[a]Laboratoire d'Enzymologie et Biochimie Structurales (LEBS), Unité Propre de Recherche 3082, Centre National de la Recherche Scientifique (CNRS), 91198 Gif sur Yvette, France; [b]Unité Micalis, Domaine de La Minière, Unité Mixte de Recherche (UMR) 1319, Institut National de la Recherche Agronomique (INRA), 78280 Guyancourt, France; and [c]Institut de Biochimie et Biophysique Moléculaire et Cellulaire (IBBMC), UMR 8619 CNRS, Université Paris-Sud 11, 91405 Orsay, France

Edited by Richard Losick, Harvard University, Cambridge, MA, and approved November 26, 2012 (received for review August 9, 2012)

The quorum-sensing regulator PlcR is the master regulator of most known virulence factors in *Bacillus cereus*. It is a helix-turn-helix (HTH)-type transcription factor activated upon binding of its cognate signaling peptide PapR on a tetratricopeptide repeat-type regulatory domain. The structural and functional properties of PlcR have defined a new family of sensor regulators, called the RNPP family (for Rap, NprR, PrgX, and PlcR), in Gram-positive bacteria. To fully understand the activation mechanism of PlcR, we took a closer look at the conformation changes induced upon binding of PapR and of its target DNA, known as PlcR-box. For that purpose we have determined the structures of the apoform of PlcR (Apo PlcR) and of the ternary complex of PlcR with PapR and the PlcR-box from the *plcA* promoter. Comparison of the apoform of PlcR with the previously published structure of the PlcR–PapR binary complex shows how a small conformational change induced in the C-terminal region of the tetratricopeptide repeat (TPR) domain upon peptide binding propagates via the linker helix to the N-terminal HTH DNA-binding domain. Further comparison with the PlcR–PapR–DNA ternary complex shows how the activation of the PlcR dimer allows the linker helix to undergo a drastic conformational change and subsequent proper positioning of the HTH domains in the major groove of the two half sites of the pseudopalindromic PlcR-box. Together with random mutagenesis experiments and interaction measurements using peptides from distinct pherogroups, this structural analysis allows us to propose a molecular mechanism for this functional switch.

crystal structure | protein–DNA interaction | quorum sensor | regulation mechanism

Communication is the essence of important biological processes in the living world. In bacteria, quorum sensing enables a population to trigger physiological processes depending on cell density (1). In Gram-positive bacteria, such as Bacilli and Cocci, new quorum-sensing regulators have been found that, unlike in most described quorum-sensing systems, are controlled by their direct interaction with a reimported signaling peptide: Rap proteins involved in the development of competence and sporulation in Bacilli (2); the necrotrophic response regulator NprR, which enables necrotrophism in *Bacillus thuringiensis* (3); the sex pheromone receptor PrgX involved in the control of conjugation in *Enterococcus faecalis* (4); and the transcription regulator PlcR responsible for the production of virulence factors in *B. thuringiensis* and *Bacillus cereus* (5). These proteins share structural similarities: tetratricopeptide repeats (TPRs) forming a peptide binding domain (6) and a helix-turn-helix (HTH) DNA-binding domain (7) in the case of transcriptional regulators. They have been grouped in a new family of quorum sensors called RNPP, for Rap, NprR, PrgX, and PlcR (8).

PlcR was first identified by Lereclus and colleagues (9) as a positive transcriptional regulator of the Phosphatidylinositol-Specific Phospholipase C gene *plcA* at the onset of the stationary phase in *B. thuringiensis*. The *plcR* gene is found in bacteria of the *B. cereus* group, which consists of several spore-forming adenine- and thymine (AT)-rich bacteria (5, 10). *plcR* codes for a 34 kDa protein that positively regulates its own expression. It was shown to be a pleiotropic regulator controlling the expression of 45 genes including virulence factors, such as enterotoxins, cytotoxins, and hemolysins (5). Virulence of a *plcR*-deficient mutant is abolished in various animal models of infection (11, 12). PlcR activates the transcription of its target genes by binding to a consensus sequence defined as wTATGnAwwwwTnCATAw (5, 13). The activity of PlcR is under the control of the signaling peptide PapR (14). *papR* belongs to the PlcR regulon and is located 70 bp downstream from *plcR*. It encodes a 48 aa peptide that is secreted and then reimported through the oligopeptide permease (OppABCDF) system (15). Once inside the cell, its processed truncated form binds PlcR and promotes its recognition of the PlcR box. The minimal active form of PapR was originally shown to be the LPFEF C-terminal pentapeptide PapR5. A more extensive study focusing on the *B. thuringiensis* 407 strain revealed that the active biological form of PapR in both intra- and extracellular environments was the C-terminal heptapeptide ADLPFEF, called PapR7 (16). The activation mechanism of PlcR by PapR has been shown to be strain specific (14). PapR sequences from different strains of the *B. cereus* group show divergences in their three N-terminal residues, whereas the PFEF core is more conserved. Analysis of a phylogenetic tree built by comparison of the amino acid sequences of PlcR and PapR from 29 different strains resulted in the definition of four groups (I to IV) of PlcR–PapR pairs corresponding to four different pherotypes in the *B. cereus* group (10). However, the structural basis for this specificity remains unknown. The crystal structure of the 34 kDa PlcR protein from group I in complex with the pentapeptide PapR5 (LPFEF) was published in 2007 (8). This binary complex is a dimer similar to the structure of the other RNPP transcriptional regulator PrgX (17). Each subunit of PlcR consists of an N-terminal HTH DNA-binding domain composed of four α-helices and a C-terminal regulatory domain composed of 10 α-helices forming five degenerated TPR motifs, each composed of a pair of antiparallel α-helices. The first helix of the TPR domain comprises an N-terminal extension forming a long helix of 30 residues spanning over 40 Å, which connects the HTH- and TPR-domains. It has been named the linker helix (8). Finally, an additional helix, designated as capping helix (8), is found at the C terminus of the protein (Fig. S1).

Author contributions: R.G., L.S., and S.N. designed research; R.G., L.S., M.N., and Y.R. performed research; R.G., L.S., M.N., D.L., and S.N. analyzed data; and R.G., L.S., D.L., and S.N. wrote the paper.

The authors declare no conflict of interest.

This article is a PNAS Direct Submission.

Data deposition: The atomic coordinates have been deposited in the Protein Data Bank, www.pdb.org [PDB ID code 4FSC (PlcR apoform) and 3U3W (PlcR/PapR7/DNA complex)].

[1]To whom correspondence should be addressed. E-mail: sylvie.nessler@u-psud.fr.

This article contains supporting information online at www.pnas.org/lookup/suppl/doi:10.1073/pnas.1213770110/-/DCSupplemental.

In this article we describe the crystal structures of PlcR in its apoform (Apo PlcR) and in complex with the physiological peptide PapR7 and DNA. Comparison of these two new structures with the previously published binary complex PlcR–PapR5 reveals a subtle effect of peptide binding and a drastic conformational change of the PlcR–PapR complex upon DNA binding. Together with the characterization of PlcR mutants active in the absence of PapR, this structural analysis allowed us to propose a molecular activation mechanism for this virulence regulator.

Results

Crystal Structure of Apo PlcR. We solved the X-ray crystal structure of the apoform of PlcR from *B. thuringiensis* strain 407 (pherogroup I) at 3.65 Å resolution, in space group $P3_1$, by molecular replacement, using monomer A of the PlcR–PapR5 binary complex (PDB ID 2QFC) (8) as the searching model. The diffraction and refinement statistics are given in Table S1. The crystallographic asymmetric unit contains four molecules, which are nearly identical with an average rmsd of 0.93 Å over an average of 262 aligned Cα atoms. There is no significant electron density for loops 16–19 and 26–31 in the HTH domain, neither for loop 55–58 connecting the HTH domain to the linker helix. Lastly, the loop 250–253 connecting helices α13–α14 of the last TPR is also disordered (Fig. S2*A*).

The four molecules of the asymmetric unit form two independent dimers. Analysis of protein–protein interactions with NOXclass (18) showed that Apo PlcR is an obligate biological dimer, characterized by a total buried surface area of about 3,150 $Å^2$ (interface area of 1,570 $Å^2$) (19). Contacts between subunits extend from the N-terminal HTH DNA-binding domain to the C-terminal TPR domain through the linker helix (Fig. 1*A*). These are mainly nonbonded hydrophobic interactions. Only four hydrogen bonds are observed between main chain atoms from the interacting loops α12–α13 and α14–α15 (Fig. 1*A*).

Comparison of Apo PlcR with the Binary Complex PlcR–PapR5. Comparison of Apo PlcR with the binary complex (PDB ID 2QFC) (8) allowed us to infer the activation mechanism of PlcR. Superposition of each PlcR monomer from both structures displayed an rmsd varying from 1.46 Å to 2.04 Å over about 240 aligned Cα atoms, depending on the considered subunits. The main difference resides in the slightly different orientations of the HTH domains and of the long linker helix α5 (Fig. S2*B*). Removing the corresponding residues from the comparative superposition of the two structures decreases the rmsd to about 0.87 Å over 207 aligned Cα atoms. In a similar manner, when comparing the dimers of Apo PlcR and of the PlcR–PapR5 complex (Fig. 1*B*), an rmsd value of about 1.3 Å over 410 aligned Cα atoms of their C-terminal domains is found. When superposing only one subunit of the dimers, a minor rotation of the second subunit is observed. It is centered on the dimerization axis formed by loop α12–α13 between the TPR-4 and TPR-5 motifs (Fig. 1*B*). As a consequence, the dimer of the binary complex PlcR–PapR5 has a reduced total buried surface area of 2,400 $Å^2$ (interface area of 1,190 $Å^2$) compared with the 3,140 $Å^2$ (interface area of 1,570 $Å^2$) observed in the Apo PlcR dimer.

We thus tried to understand how peptide binding induces this conformational change. A more careful comparison of the peptide-binding groove in the two PlcR structures revealed that binding of PapR induces a minor shift of the capping helix α15 (Fig. 1*B*). As a consequence, the loop α14–α15, which is involved in dimer contacts with the neighboring helix α12 (Fig. 1*A*), is also slightly shifted, inducing the rotation of the neighboring subunit around the α12–α13 contact region (Fig. 1*B*). At the opposite extremity of the protein, this small rotation results in the loss of interactions between residues from the N-terminal end of the linker helix from both subunits. In particular, a strong stacking interaction observed in Apo PlcR between the Tyr64 side-chains from each subunit is lost in the binary complex, with the distance between the two aromatic rings increasing from about 4.5 Å to 9.5 Å, respectively (Fig. 1 *C* and *D*). In the Apo form, the HTH domains of both subunits interact via their α4 helices (Fig. 1*A*), resulting in an incompatible orientation of helix α3 for DNA binding. The loss of contacts between the linker helices upon peptide binding most probably unlocks the N-terminal HTH-domains, promoting their flexibility, hence allowing DNA binding.

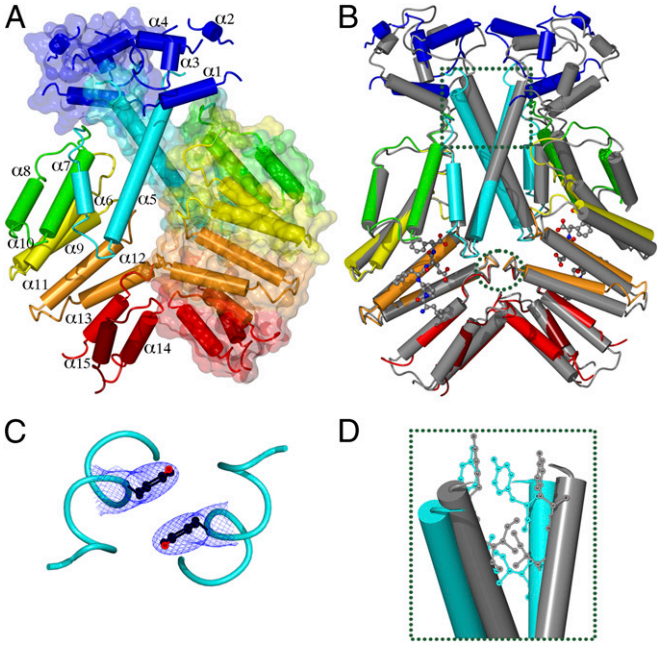

Fig. 1. Apo PlcR dimer. (*A*) Both subunits are represented in cartoon and one as surface. The N-terminal HTH domain is colored in dark blue. The TPR motifs are colored in rainbow from TPR-1 in cyan to TPR-5 in red. The N-terminal extension of the first helix α5 of TPR1 (linker helix) is shown in cyan. The C-terminal capping helix is in dark red. (*B*) Superposition of the Apo PlcR dimer (colored as in *A*) with the binary complex PlcR–PapR5 (in gray). The bound peptide is shown as a ball-and-stick model colored by atom type. The dimer contact region is highlighted with a green circle. The superposition was done using the TPR domain of one subunit. (*C*) Close view of the stacking interaction between the side chains of residues Tyr64 (in ball-and-stick) with their electron density map (2Fo-Fc) contoured at 1.0 sigma. (*D*) Detail of Fig. 1*B* (green square) centered on the linker helices. The distance between the two Tyr64 symmetrical residues increases from about 4.5 Å to 9.5 Å upon peptide binding. The two Ile68 symmetrical residues are about 5 Å apart in both structures.

This analysis suggests that in the absence of peptide, PlcR would not be able to bind DNA. This is in agreement with previous results from DNA footprinting experiments (14) and has been confirmed here by isothermal titration calorimetry (ITC) measurements showing that the presence of PapR is required to allow binding of PlcR to DNA (Fig. S3*A*). Together with functional assays demonstrating that the presence of the peptide is required for PlcR transcriptional activity (14), these results demonstrate that the activation mode of the peptide relies on subtle conformational changes.

Crystal Structure of the Ternary Complex PlcR–PapR–DNA. Crystals were obtained by mixing PlcR with the PapR7 heptapeptide (ADLPFEF) and an 18-base-pair-long dsDNA corresponding to the PlcR-box of the *plcA* promoter (5′-ctatgcaatatttcatat-3′), called *plcA*18. The crystals of the PlcR–PapR7–*plcA*18 ternary complex diffracted up to a resolution of 2.4 Å in space group $P2_1$. Calculation of the Matthews coefficient (20) suggested two molecules per asymmetric unit. The structure was solved by molecular replacement using one subunit of the PlcR–PapR5 binary complex (8) as the initial model. The dsDNA fragment was built manually. The diffraction and refinement statistics are given in Table S1.

The final model consists of a dimer of PlcR containing 280 amino acid residues and one bound PapR7 (ADLPFEF) peptide per chain, a *plcA*18 dsDNA fragment, and 255 water molecules (Fig. 2*A*). All residues of the protein are in well-defined electron density and the two subunits of PlcR are nearly identical with a low rmsd of 0.135 Å over 280 aligned Cα atoms. Analysis of protein–protein interactions with NOXclass (18) confirms that the ternary complex is an obligate biological dimer with a total buried surface area between the two protein subunits of 3,870 Å^2 (interface area of 1,934 Å^2) (19).

Peptide-Binding Mode. Clear electron density corresponding to the PapR7 heptapeptide is visible in both TPR peptide-binding domains of the ternary complex (Fig. S4*A*). The peptide is bound in a deep cleft with its C terminus buried at the bottom of the cleft (Fig. 2*B*). The contacts between the peptide and the protein are conserved in both subunits (Fig. S4*B*). The hydrophobic side chains from the peptide are involved in nonbonded interactions with the protein. Both PapR7 phenylalanines are located in hydrophobic pockets. Most hydrogen bonds are made between atoms from the peptide backbone and side chains from the protein. The only specific interactions are made between the glutamate of PapR7 and residues Lys89, Gln237, and Tyr275 of PlcR. The two additional N-terminal residues A–D of PapR7 point toward the solvent. Their presence increases the total buried surface area between the peptide and a subunit of PlcR from 629.2 Å^2 to 730.5 Å^2 in the PlcR–PapR5 (PDB ID 2QFC) and PlcR–Papr7 complexes, respectively. This observation is in agreement with ITC experiments showing that PlcR displays a slightly better affinity for PapR7 than for PapR5, with K_d values of 30 nM and 85 nM, respectively (Fig. S3 *B* and *C*). It also explains why both forms of the peptide similarly activate PlcR (8, 16).

DNA-Binding Mode. The PlcR dimer binds to the major grooves of the designed PlcR box of its regulated gene *plcA* through its HTH domains (Fig. 2*C*). Analysis of the complex formed between the protein and the *plcA*18 double-stranded oligonucleotide showed that the total surface area buried in this interaction covers 2,870 Å^2. The bound DNA fragment displays the characteristic shape of a right-handed B-form nucleic acid structure (21), with a deviation from the regular linear helix of only 3.18°. As typically observed in HTH–DNA interactions (22), the recognition helix α3 from each HTH domain is oriented almost perpendicularly to the DNA axis and specifically interacts with conserved base pairs from the major groove via the side chains of residues Gln31, Ser32, and Arg36 (Fig. S4*C*). Because the PlcR-box is not a perfect palindrome, the interactions network is not exactly the same in the two half sites. The interaction between Gln31 and base A3 is observed in both half sites. Arg36 from both subunits interact with base G5, but only one interacts with base T13 as well. Ser32 interacts via its side chain with base C14 in only one of the binding sites. These specific interactions mostly involve conserved base pairs of the PlcR-box characterized by the consensus sequence wTATGnAwwwwTnCATAw (5, 13). Nonspecific interactions between the HTH domains and the sugar-phosphate backbone of the DNA further stabilize the complex (Fig. S4*C*).

Comparison of the PlcR Binary and Ternary Complexes. A drastic reorientation of the HTH domains is observed when comparing the PlcR–PapR7–*plcA*18 ternary complex with the structures of the PlcR–PapR5 (8) binary complex (Fig. 3*A*). DNA binding induces an abrupt kink in the middle of the linker helices, which bend the N terminus by about 90° (Fig. 3*B*). This results in the making of helix α5′ (Fig. S1) and a more canonical TPR-1 motif (helices α5 and α6). Superposition of the TPR domain of one subunit from each complex outputs an rmsd of 1.3 Å over 186 aligned Cα atoms (Fig. S2*C*), demonstrating that the conformation of the TPR peptide-binding domain is not greatly affected by DNA binding. It is clear, however, that the abrupt conformational change of the linker helices and the reorientation of the HTH domains promote important changes in the dimerization mode of PlcR. Superposition of the dimers of both structures displays a high rmsd of about 3.0 Å over 325–375 aligned Cα atoms. DNA binding induces a shift of each HTH domain toward the TPR domain of the neighboring subunit, which results in the rotation of the two subunits around the dimerization axis located in the contact region involving loops α12–α13 (Figs. 1*B* and 3*A*). The total buried surface area of the PlcR dimer increases from 2,400 Å^2 on the binary complex to 3,870 Å^2 in the ternary complex, mainly due to novel contacts amid HTH domains and between the HTH domain from one subunit and the TPR domain from the next.

Our structural analysis thus shows that the subtle conformational changes induced by peptide binding allow the protein to switch from a locked-inactive conformation to a more flexible unlocked-active conformation able to undergo a large conformational change upon DNA binding.

Characterization of Constitutively Activated PlcR. To learn more about the activation mechanism of PlcR, we performed a random mutagenesis of the *plcR* gene and screened for PlcR mutants active in the absence of peptide. Plasmids harboring mutated versions of *plcR* were introduced in strain *B. thuringiensis* 407

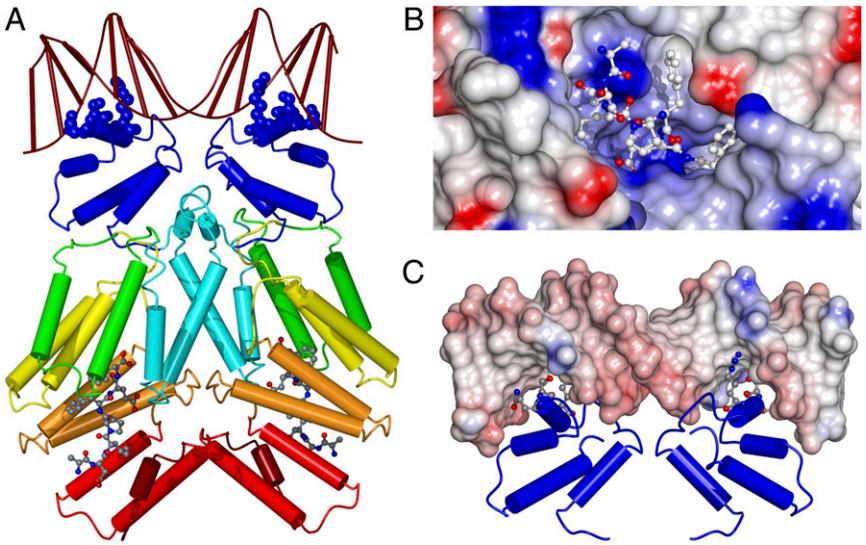

Fig. 2. Ternary complex PlcR–PapR7–*plcA*18. (*A*) The PlcR dimer is shown in cartoon colored as in Fig. 1*A*. The bound PapR7 peptide (ADLPFEF) is represented as a ball-and-stick model colored by atom type. The bound *plcA*18 DNA fragment (5′-ctatgcaatatttcatat-3′) is shown as worm and sticks colored in dark red. Residues Gln31, Ser32, and Arg36 directly involved in DNA binding are illustrated as spheres, colored in blue. (*B*) Electrostatic potential surface representation of the TPR domain of one subunit of the ternary complex following the typical charge color-code (negative, red; positive, blue; neutral, white) with the bound PapR7 represented as a ball-and-stick model colored by atom type. (*C*) Electrostatic potential surface representation of the *plcA*18 DNA bound to the HTH domains of the PlcR dimer represented in cartoon and colored in blue. Residues Gln31, Ser32, and Arg36, which bind the major grooves of DNA, represented as a ball-and-stick model.

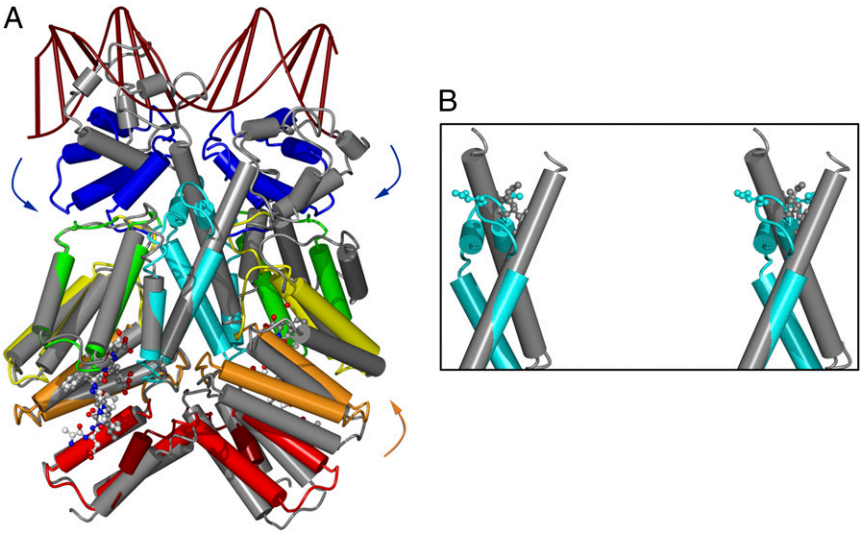

Fig. 3. Comparison of the binary and ternary complexes of PlcR. (*A*) Superposition of the ternary complex PlcR–PapR7–*plcA*18 (colored as in Fig. 2*A*) with the binary complex PlcR–PapR5 (in gray). Both models are represented in cartoon. The bound peptide in each structure is shown in ball-and-stick colored by atom type (PapR7 in white, PapR5 in gray). (*B*) Stereo-view of the superposed linker helices in the kink area. The side chains of residues Ile68 from both dimers are shown in spheres (colored as in Fig. 3*A*). The distance between the two Ile68 symmetrical residues increases from about 5 Å to 27 Å in the binary and ternary complexes, respectively.

Δ*plcRpapR plcA'lacZ* lacking PlcR and PapR and carrying a transcriptional fusion between the promoter of *plcA* and the *lacZ* reporter gene. The *plcA* gene is under the direct control of PlcR, and activation of its promoter directly reflects activity of the PlcR protein. One clone in particular showed a strong induction of the reporter gene. PlcR activity in this clone was evaluated using β-galactosidase assays (Fig. 4*A*, lane 3). The activity of the mutant is similar to the activity of the wild-type PlcR–PapR complex. Mutations in the *plcR* gene were identified by sequencing and translated to I68N/L185S/M272T. Subsequent functional characterization of the proteins carrying single mutations revealed that I68N is necessary and sufficient for PlcR activity in the absence of PapR (Fig. 4*A*, lanes 4–6). In parallel, we introduced the Y64A mutation in PlcR. This mutant presented a slightly higher activity compared with that of wild-type PlcR (Fig. S5*A*) in the absence of peptide, confirming the importance of this structurally identified residue (Fig. 1*B*) in the activation mechanism. However, this mutation had a much weaker effect than I68N on the activity of PlcR. ITC experiments showed that PlcR (I68N) binds PapR7 with a strong affinity (K_d = 6 nM) (Fig. S5*B*). They also confirmed that the mutant PlcR (I68N) binds DNA almost as efficiently in the presence of peptide (Fig. S5*C*) as in its absence (Fig. S5*D*), whereas the wild-type PlcR requires the presence of PapR to bind DNA (Fig. S3*A*). Interestingly, the ITC signal is exothermic with the I68N mutant protein and endothermic with wild-type PlcR. The large conformational change observed upon DNA binding could explain the positive enthalpy change (ΔH) displayed by the wild-type protein. The mutant protein in turn is most probably in the active conformation characterized by the broken linker helix, and the negative ΔH directly reflects the favorable protein–DNA interaction.

These results demonstrate that it is possible to activate PlcR in the absence of peptide by a single amino acid substitution located in an essential area of the protein structure—that is, the kink region of the linker helix (Fig. 3). In a similar way to peptide binding, mutations I68N and to a lower extent Y64A increase the flexibility of PlcR and promote an active conformation of the protein compatible with DNA binding.

Specificity Assays. It has been shown that PlcR from the phylogenetic group I, the focus of our study, is activated by its cognate heptapeptide PapR-I (ADLPFEF), but can also be partially activated by PapR-II (SDMPFEF) and to a lesser extent by PapR-IV (SDLPFEH) but not by PapR-III (NEVPFEF) (16). To elucidate which part of the bound peptide is directly involved in the activation process, we compared the affinity of these three peptides for PlcR-I with that of its cognate peptide PapR-I. ITC measurements demonstrated that PapR-II displays a K_d of 77 nM of the same order as the reference K_d value of 30 nM observed for PapR-I. However, the PapR-III and PapR-IV peptide have a strongly decreased affinity with K_d values of 0.97 μM and 1.1 μM, respectively (Fig. S6). Because the pentapeptide (LPFEF) has been shown to activate PlcR-I almost as efficiently as the heptapeptide (ADLPFEF) (16), we can assume that the two first residues of the latter are not crucial for the activation of the protein. The third residue is then the only difference that could explain why PapR-III is inactive and PapR-II is active. Having a short apolar residue V at this position instead of the L residue found in PapR-I impairs the activation, whereas its substitution into a longer M residue in PapR-II only promotes its decrease. The poor affinity of PapR-IV can be explained by the substitution of the conserved PFEF motif into PFEH, which introduces a polar charged histidine residue in the hydrophobic pocket of the last phenylalanine residue. This clearly demonstrates that the conserved PFEF motif is essential for peptide binding. It also suggests that the L residue preceding this motif might be directly involved in the activation mechanism. This hypothesis is supported by our structural study showing that the

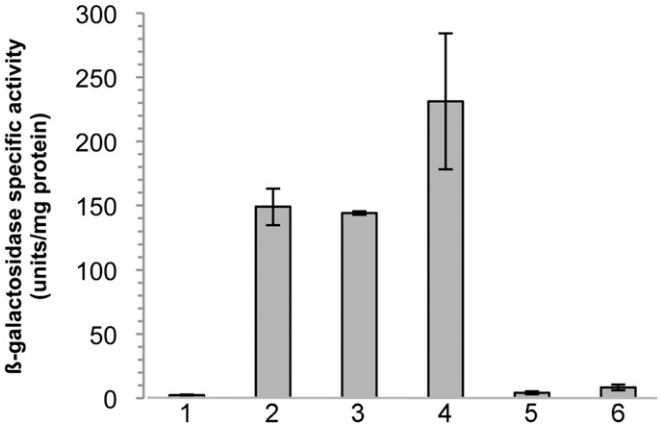

Fig. 4. Characterization of the PlcR(I68N) mutant protein. β-galactosidase was assayed on cells Bt407 Δ*plcRpapR plcA'lacZ* carrying pHT304.18-Pxyl with each gene of interest: *plcR*, $plcR_{I68N/L185S/M272T}$, $plcR_{I68N}$, $plcR_{L185S}$, or $plcR_{M272T}$ sampled at the beginning of stationary phase. PapR7 was added to the culture of cells producing PlcR-wt at the time of inoculation. The bars are labeled 1–6 corresponding to 1, $PlcR_{wt}$; 2, $PlcR_{wt}$ + PapR7; 3, $PlcR_{I68N/L185S/M272T}$; 4, $PlcR_{I68N}$; 5, $PlcR_{L185S}$; 6, $PlcR_{M272T}$. The results are the mean values of two independent experiments, and error bars represent SDs.

side chain of the L residue of the peptide is bound in a hydrophobic pocket formed by PlcR residues Tyr275 and Ala278 from the C terminus capping helix and Tyr240 from TPR-5 (Fig. S7), a region of the protein that has been shown to be involved in the global conformational change induced by peptide binding.

Discussion

Activation Mode of PlcR. Much speculation has surrounded the activation mode of PlcR, and understanding how PapR activates this transcription factor has been quite a challenge. It has been shown that PlcR is not active in the absence of peptide (14, 16). Directed mutagenesis of Tyr275, involved in peptide binding, to alanine promoted a twofold increase in PlcR activity after addition of PapR (16). Tyr275 is located on the C-terminal capping helix and specifically interacts with the side chain of the E residue of the ADLPFEF peptide. The authors suggested that PapR may enhance the TPR modifications necessary for activation by slightly pulling the PlcR C-terminal capping helix toward the center of the molecule (16). Comparison of the PlcR–PapR5 binary complex with our structure of Apo PlcR confirms this subtle movement of the α15 capping helix and reveals that it propagates to helix α14 from the TPR-5 motif, which is directly involved in dimerization. Peptide binding destabilizes the contact region of the dimer, inducing a small rotation around loop α12–α13, preceding TPR-5. At the N-terminal extremity of the PlcR dimer, this minor rotation results in the loss of interactions between residues Tyr64 of the linker helices from both subunits. Our structure of the ternary complex PlcR–PapR7–*plcA*18 shows that, in the presence of DNA, the gain of flexibility induced by peptide binding allows the long linker helices to break in two individual helices for proper reorientation of the HTH domains toward the major grooves of the DNA binding sites. The break point of the linker helix corresponds to residue Ile68, which mutation to asparagine has been shown to result in a constitutively active mutant protein. Due to the emergence of more favorable polar interactions with neighboring residues from the same chain, this substitution most probably destabilizes the stacking interaction with the symmetrical residue, weakening the dimer contacts in the N-terminal region and leading directly to the active conformation.

Finally, we propose an activation mechanism in two steps. The dimeric form of PlcR is double-locked in an inactive conformation due to the stacking interactions of Ile68 and Tyr64 with their symmetrical counterparts (Fig. 1*D*). Upon peptide binding, the change in the dimer contacts opens the first lock, formed by the interaction between the two Tyr64 residues. This results in a weakened active form of the protein. The second lock formed by the stacked Ile68 side chains is then free to unlock upon DNA binding (Fig. 3*B*). Hence, these two key residues function as a double-lock system, which is unlocked in two sequential steps, each corresponding to the loss of stacking interactions of Tyr64 and Ile68, respectively (Fig. 5).

Specificity of Activation. Our structural study clearly shows that the side chain of the L residue of PapR is bound in a hydrophobic pocket formed by PlcR residues from the C-terminal dimerization region. Its interaction with Ala278 is in agreement with previous results showing that these two residues (L in PapR and Ala278 in PlcR) determine the specificity of the PlcR–PapR complex (10). This suggests that the L residue could directly trigger the conformational change that promotes PlcR activation. Our specificity assays showing that the weaker activating effect of PapR-II is not due to poor binding but to the L to M substitution further emphasized the strategic role played by the peptide residue in the third position. Taken together these structural and functional results suggest that the L residue in the third position of PapR7-I is the key residue triggering the molecular mechanism of the PlcR-I activation process.

Conservation of the Activation Mode in the RNPP Family. The RNPP effector PrgX of *Enterococcus faecalis* presents the highest structural similarity with the dimer of PlcR. Apo PrgX is a stable tetramer formed by two tail-to-tail bound PlcR-like dimers that repress the *prgQ* promoter by cooperatively binding on two operator sites. The binding of the sex pheromone cCF10 weakens the stability of the tetramer and reduces the affinity of the protein toward the second operator, thus activating the expression of the *prgQ* operon. The iCF10 inhibitory peptide binds in the same pocket of the TPR domain as cCF10, but it does not promote the activating conformational change (17, 23). As described previously (8), PlcR and PrgX share a similar binding mode, although the effect of peptide binding is quite different.

Regarding the other members of the RNPP family, both structures of RapH (24) and RapF (25) have been obtained in complex with their respective protein targets, Spo0F and ComAc, in the absence of their cognate inhibitory Phr peptides. The regulatory mechanism of the Rap proteins by Phr peptides is therefore unknown. In these proteins, the DNA-binding domain is replaced by a Rap-specific N-terminal domain consisting of a three-helix bundle, which is involved in binding of the protein target. The TPR domains, however, are conserved in comparison with PlcR and PrgX, and residues potentially involved in binding of the Phr peptides have already been identified. The role of a conserved asparagine has also been highlighted (26). Binding of Phr peptides thus most probably induces a conformational change that propagates from the TPR domain to the N-terminal domain interacting with the targeted protein. The molecular mechanism of the peptide-dependent regulation mode of the RNPP proteins is, however, specific to each member of the family and the Rap inhibition mechanism cannot be deduced from the mechanisms described for PrgX or PlcR.

Toward New Antimicrobial Agents. Since the characterization of the RNPP family, a rapid increase of the number of sensor regulators uncovered within the low GC percent Gram-positive bacteria was

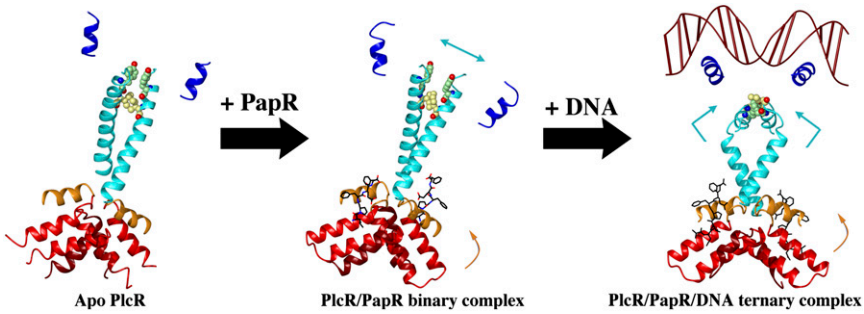

Fig. 5. PlcR activation mechanism. In this model, the regions of the PlcR dimer with the most important changes amid the three states of the protein are shown (same orientation upon superposition of the TPR domain of subunit A). In the first step, peptide (in black sticks) binding induces a small reorientation (orange arrow) of the C-terminal helices from the TPR domains involved in dimer contacts: helices α12 (in orange), α13–α14 (in red), and the capping helix (in dark red). This conformational change propagates along the structure to the linker helix α5 (in cyan), resulting in the loss of the stacking interaction between residues Tyr64 (green spheres) and the reduction of the interface area between the HTH domains and the linker region (cyan arrow). In the second step, DNA binding (in dark red) promotes a drastic kink in the linker helix (cyan arrows) by breaking the weakened stacking interaction between residues Ile68 (yellow spheres). This striking conformational change results in significant changes in the dimerization mode of the TPR domains (orange arrow) and allows helix α3 of both HTH domains to fit in the two half sites of the bound DNA.

observed, pointing out their important role in adaptative and virulence processes (27–32). This clearly identifies these regulators as major targets for the search of new molecules with applications in medical, food, and biotechnology areas. The precise understanding of the mode of activation of the RNPP regulators will provide necessary insights for designing quorum-quenching molecules useful as antimicrobial drugs, decontaminating agents or activators of expression of genes of interest.

Materials and Methods

Samples Preparation. *B. thuringiensis* 407 wild-type and mutant PlcR proteins were overexpressed as a C-terminal His6-tagged recombinant protein in *Escherichia coli* strain C41 (DE3) (Invitrogen) and purified by a two-step purification procedure (immobilized-metal affinity and size exclusion chromatography). Details of the expression and purification protocols are given in *SI Materials and Methods*. Preparation of dsDNA fragments containing the PlcR-box of the *plcA* gene and used for ITC experiments, cocrystallization assays, and mutagenesis experiments is detailed in *SI Materials and Methods*, as well as the protocol used for the preparation of the PapR peptides.

Crystallographic Analysis. Apo PlcR was crystallized at a concentration of 4 mg/mL in a solution containing 0.1 M sodium chloride, 0.1 M trisodium citrate pH 5.6, 40% (vol/vol) PEG 400 with a protein–reservoir solution ratio of 1:2. The PlcR–PapR7–*plcA*18 ternary complex crystallized in a condition containing 0.16 M calcium acetate, 0.08 M sodium cacodylate pH 5.6, 8% (wt/vol) PEG 8000 and 5% (vol/vol) glycerol with a protein–reservoir solution ratio of 1:2. More details on the crystallization experiments are given in *SI Materials and Methods*. X-ray diffraction data of Apo PlcR were recorded at the SOLEIL synchrotron beamline PROXIMA 1. The dataset of the ternary complex was collected at the ESRF synchrotron beamline ID29 (Grenoble, France). Details of diffraction data collection and processing as well as structure refinement procedures are given in *SI Materials and Methods*. Final statistics are listed in Table S1.

Structural Coordinates and Figures. The coordinate and structure factors of the apoform of PlcR and of the ternary complex PlcR–PapR7–*plcA*18 have been deposited with the Protein Data Bank (RCSB PDB) under the ID codes 4FSC and 3U3W, respectively. All structural figures were created with CCP4MG (33). Electrostatic potential surfaces were calculated by the Poisson–Boltzmann solver within CCP4MG and colored accordingly.

ITC. Affinities of PlcR to PapR5, PapR7, noncognate peptides, and selected dsDNA were measured by ITC at 20 °C. The dissociation constant K_d was calculated using the "One Set of Sites" curve-fitting model. Details of the measurement protocols are given in *SI Materials and Methods*.

Mutational Analysis. For the isolation of PlcR mutants active without PapR, random mutagenesis was achieved by amplifying the *plcR* gene by PCR with Standard Taq polymerase using *B. thuringiensis* 407 chromosomal DNA as template and primers plcRa3 and plcRmuta (Table S2). Single mutations were introduced in the coding sequence of *plcR* by directed PCR mutagenesis. More details are given in *SI Materials and Methods*.

Beta-Galactosidase Activity Assays. Cells were prepared as described in *SI Materials and Methods*. A total of 5 μM PapR7 was added at the start of the culture when stated. β-galactosidase assays were performed as described previously (29).

ACKNOWLEDGMENTS. We thank staff of beamlines Proxima-1 and ID19 at the synchrotron radiation facilities SOLEIL and ESRF, respectively. We also acknowledge the use of the Imagif crystallization platform. This work was supported by grants from the Centre National de la Recherche Scientifique, the Institut National de la Recherche Agronomique, and the French Agence Nationale de la Recherche (ANR-09-BLAN-0253).

1. Waters CM, Bassler BL (2005) Quorum sensing: Cell-to-cell communication in bacteria. *Annu Rev Cell Dev Biol* 21:319–346.
2. Bongiorni C, Ishikawa S, Stephenson S, Ogasawara N, Perego M (2005) Synergistic regulation of competence development in *Bacillus subtilis* by two Rap-Phr systems. *J Bacteriol* 187(13):4353–4361.
3. Dubois T, et al. (2012) Necrotrophism is a quorum-sensing-regulated lifestyle in *Bacillus thuringiensis*. *PLoS Pathog* 8(4):e1002629.
4. Bae T, Clerc-Bardin S, Dunny GM (2000) Analysis of expression of prgX, a key negative regulator of the transfer of the *Enterococcus faecalis* pheromone-inducible plasmid pCF10. *J Mol Biol* 297(4):861–875.
5. Agaisse H, Gominet M, Okstad OA, Kolstø AB, Lereclus D (1999) PlcR is a pleiotropic regulator of extracellular virulence factor gene expression in *Bacillus thuringiensis*. *Mol Microbiol* 32(5):1043–1053.
6. Blatch GL, Lässle M (1999) The tetratricopeptide repeat: A structural motif mediating protein-protein interactions. *Bioessays* 21(11):932–939.
7. Wintjens R, Rooman M (1996) Structural classification of HTH DNA-binding domains and protein-DNA interaction modes. *J Mol Biol* 262(2):294–313.
8. Declerck N, et al. (2007) Structure of PlcR: Insights into virulence regulation and evolution of quorum sensing in Gram-positive bacteria. *Proc Natl Acad Sci USA* 104(47):18490–18495.
9. Lereclus D, Agaisse H, Gominet M, Salamitou S, Sanchis V (1996) Identification of a *Bacillus thuringiensis* gene that positively regulates transcription of the phosphatidylinositol-specific phospholipase C gene at the onset of the stationary phase. *J Bacteriol* 178(10):2749–2756.
10. Slamti L, Lereclus D (2005) Specificity and polymorphism of the PlcR-PapR quorum-sensing system in the *Bacillus cereus* group. *J Bacteriol* 187(3):1182–1187.
11. Salamitou S, et al. (2000) The *plcR* regulon is involved in the opportunistic properties of *Bacillus thuringiensis* and *Bacillus cereus* in mice and insects. *Microbiology* 146(Pt 11):2825–2832.
12. Callegan MC, et al. (2003) Relationship of *plcR*-regulated factors to *Bacillus endophthalmitis* virulence. *Infect Immun* 71(6):3116–3124.
13. Gohar M, et al. (2008) The PlcR virulence regulon of *Bacillus cereus*. *PLoS ONE* 3(7):e2793.
14. Slamti L, Lereclus D (2002) A cell-cell signaling peptide activates the PlcR virulence regulon in bacteria of the *Bacillus cereus* group. *EMBO J* 21(17):4550–4559.
15. Gominet M, Slamti L, Gilois N, Rose M, Lereclus D (2001) Oligopeptide permease is required for expression of the *Bacillus thuringiensis plcR* regulon and for virulence. *Mol Microbiol* 40(4):963–975.
16. Bouillaut L, et al. (2008) Molecular basis for group-specific activation of the virulence regulator PlcR by PapR heptapeptides. *Nucleic Acids Res* 36(11):3791–3801.
17. Shi K, et al. (2005) Structure of peptide sex pheromone receptor PrgX and PrgX/pheromone complexes and regulation of conjugation in *Enterococcus faecalis*. *Proc Natl Acad Sci USA* 102(51):18596–18601.
18. Zhu H, Domingues FS, Sommer I, Lengauer T (2006) NOXclass: Prediction of protein-protein interaction types. *BMC Bioinformatics* 7:27.
19. Krissinel E, Henrick K (2007) Inference of macromolecular assemblies from crystalline state. *J Mol Biol* 372(3):774–797.
20. Matthews BW (1968) Solvent content of protein crystals. *J Mol Biol* 33(2):491–497.
21. Zheng G, Lu XJ, Olson WK (2009) Web 3DNA—A web server for the analysis, reconstruction, and visualization of three-dimensional nucleic-acid structures. *Nucleic Acids Res* 37(Web Server issue):W240–W246.
22. Brennan RG, Matthews BW (1989) The helix-turn-helix DNA binding motif. *J Biol Chem* 264(4):1903–1906.
23. Kozlowicz BK, et al. (2006) Molecular basis for control of conjugation by bacterial pheromone and inhibitor peptides. *Mol Microbiol* 62(4):958–969.
24. Parashar V, Mirouze N, Dubnau DA, Neiditch MB (2011) Structural basis of response regulator dephosphorylation by Rap phosphatases. *PLoS Biol* 9(2):e1000589.
25. Baker MD, Neiditch MB (2011) Structural basis of response regulator inhibition by a bacterial anti-activator protein. *PLoS Biol* 9(12):e1001226.
26. Diaz AR, et al. (2012) *Bacillus subtilis* RapA phosphatase domain interaction with its substrate, phosphorylated Spo0F, and its inhibitor, the PhrA peptide. *J Bacteriol* 194(6):1378–1388.
27. Fleuchot B, et al. (2011) Rgg proteins associated with internalized small hydrophobic peptides: A new quorum-sensing mechanism in streptococci. *Mol Microbiol* 80(4):1102–1119.
28. Fontaine L, et al. (2010) A novel pheromone quorum-sensing system controls the development of natural competence in *Streptococcus thermophilus* and *Streptococcus salivarius*. *J Bacteriol* 192(5):1444–1454.
29. Perchat S, et al. (2011) A cell-cell communication system regulates protease production during sporulation in bacteria of the *Bacillus cereus* group. *Mol Microbiol* 82(3):619–633.
30. Chang JC, LaSarre B, Jimenez JC, Aggarwal C, Federle MJ (2011) Two group A streptococcal peptide pheromones act through opposing Rgg regulators to control biofilm development. *PLoS Pathog* 7(8):e1002190.
31. Zheng F, et al. (2011) Contribution of the Rgg transcription regulator to metabolism and virulence of *Streptococcus suis* serotype 2. *Infect Immun* 79(3):1319–1328.
32. Shelburne SA, 3rd, et al. (2011) An amino-terminal signal peptide of Vfr protein negatively influences RopB-dependent SpeB expression and attenuates virulence in *Streptococcus pyogenes*. *Mol Microbiol* 82(6):1481–1495.
33. Potterton L, et al. (2004) Developments in the CCP4 molecular-graphics project. *Acta Crystallogr D Biol Crystallogr* 60(Pt 12 Pt 1):2288–2294.